Chapter 4
Stable Levitation

Chengqian Zhang, Zhezai Hu, Jun Xie, and Peng Zhao

4.1 Introduction

Earnshaw's Theorem, formulated by Samuel Earnshaw, serves as a foundational principle within classical mechanics [1, 2], positing the impossibility of point particles achieving stable equilibrium solely under classical inverse square law forces. This theorem resonates throughout the realms of physics, rendering stable suspension unattainable through gravity, electrostatics, and static magnetism. At its core lies the interplay of electric field line divergence and Gauss's law, resulting in the absence of stable equilibria in open spaces. The electric force derived from potential adheres mathematically to Laplace's equation, a perpetually divergence-free framework.

The theorem's significance reverberates in multi-particle scenarios, precluding stable configurations. Demonstrated by contradiction, equilibrium configurations teeter into instability due to potential energy extremities. Its implications span domains such as electric dipole orbits, and it curtails applications of static magnetic fields for levitation due to the inverse cube relationship.

A pivotal moment transpired in 1939 when German physicist Braunbeck defied this constraint, achieving stable levitation using diamagnetic materials. This breakthrough laid the foundation for the emergence of Magneto-Archimedes levitation, introduced by Yasuhiro Ikezoe in 1998 [3]. This technique amplifies buoyancy and magnetic forces by manipulating paramagnetic medium pressure, favoring permanent magnets over electromagnets. This chapter probes the equilibrium interplay, ranging from diamagnetic achievements to the technological leaps of Magneto-Archimedes levitation [4, 5].

C. Zhang (✉) · Z. Hu · P. Zhao
The State Key Laboratory of Fluid Power and Mechatronic Systems, College of Mechanical Engineering, Zhejiang University, Hangzhou, China
e-mail: zhangcq@zju.edu.cn

J. Xie
College of Mechanical Engineering, Zhejiang University of Technology, Hangzhou, China

The Magneto-Archimedes levitation method, an extraordinary feat within magnetic levitation, offers precise manipulation and analysis of objects suspended within paramagnetic mediums. Orchestrating magnetic buoyancy and gravitational forces, this method presents a captivating means of suspending and positioning objects without physical touch. This paper delves into the nuanced intricacies of the Levitation Feature, delving into vital aspects like Levitation Height [6, 7] and Levitation Posture. Furthermore, it introduces the groundbreaking concept of Circular Levitation, expanding stability beyond the central axis. This innovation holds promise across diverse applications, encompassing density measurements, defect detection, and beyond.

4.2 Earnshaw's Theorem

Earnshaw's theorem, named after Samuel Earnshaw, is a fundamental theorem in classical mechanics that states that a collection of point particles cannot be maintained in a stable equilibrium solely by the interaction forces governed by the classical inverse square law, i.e., a mechanical equilibrium structure composed solely of gravitational, electrostatic, and static magnetic forces cannot achieve stable suspension. The theorem states that there is no configuration of the particles that results in a stable equilibrium, i.e., a configuration where the forces on each particle sum to zero.

The behavior of a point charge in a static electric field can be explained by considering Gauss's law. In order for a particle to be in a stable equilibrium, small disturbances or "pushes" in any direction should not disrupt the equilibrium; the particle should return to its original position. This implies that the electric field lines surrounding the equilibrium position of the particle should all point inward, towards that position. If all the field lines around the equilibrium point converge towards it, then the divergence of the field at that point must be negative, indicating that it acts as a sink.

However, Gauss's law dictates that the divergence of any electric field in free space is zero. Therefore, in mathematical terms, any electrical force (F) resulting from a potential (U) will always satisfy Laplace's equation, guaranteeing that it is divergenceless.

$$\nabla \cdot \boldsymbol{F} = -\nabla^2 U = 0 \qquad (4.1)$$

In free space, the absence of local minima or maxima in the field potential is due to the fact that there are only saddle points. This implies that a stable equilibrium for a particle cannot exist, and there must be an instability in at least one direction. However, it is important to note that this argument may not be sufficient if all the second derivatives of the potential function, denoted as U, are null. In such cases, additional considerations are required to determine the stability of the system.

To comprehend Earnshaw's theorem, it is beneficial to examine a system comprising two charged particles. The interactions between these particles adhere to

Coulomb's law, which asserts that the force between two charged particles is directly proportional to the product of their charges and inversely proportional to the square of the distance separating them. When the two particles possess identical charges, they will repel each other. Conversely, if they bear opposite charges, they will attract each other. Upon attempting to establish a state of equilibrium by countering the forces between the particles, we discover that a stable equilibrium is unattainable.

Earnshaw's theorem was proven using the method of contradiction. Assume that a stable equilibrium configuration exists for a collection of point particles. By definition, the equilibrium configuration is one where the forces on each particle sum to zero. If we consider the second derivative of the potential energy with respect to the position of each particle, Earnshaw showed that this equilibrium configuration is necessarily a local maximum or a local minimum of the potential energy, but not a stable equilibrium. In other words, any small perturbation from the equilibrium configuration will result in the particles moving away from the equilibrium position, and the system will be unstable. Earnshaw's theorem has important implications in various areas of physics. For example, it has been used to prove that there can be no stable orbits of charged particles around a static electric dipole. This is because the forces between the charged particles fall off as the inverse square of the distance, which violates the conditions for stable equilibrium. The theorem also places a fundamental limitation on the use of static magnetic fields for levitation. This is because, as stated earlier, the forces between magnetic dipoles fall off as the inverse cube of the distance, which violates the conditions for stable equilibrium.

An intriguing implication of Earnshaw's theorem is its essential restriction on the practical application of static magnetic fields for levitation purposes. As previously mentioned, the forces between magnetic dipoles decline in proportion to the inverse cube of the distance, thereby contradicting the conditions required for stable equilibrium. However, in 1939, German physicist Braunbeck managed to achieve stable levitation within a static magnetic field by utilizing diamagnetic materials with negative magnetic susceptibility. This breakthrough not only provided a supplementation to Earnshaw's theorem but also paved the way for the advancement of diamagnetic levitation technology.

Diamagnetic levitation relies on the fact that the magnetic susceptibility of diamagnetic materials is negative, which means that they are repelled by magnetic fields. This repulsion results in a force that can balance the force of gravity, allowing the diamagnetic material to levitate stably in a magnetic field. The force of the magnetic field on a diamagnetic material is given by:

$$F = -\chi V \nabla B^2 / (2\mu_0) \qquad (4.2)$$

where χ is the magnetic susceptibility of the material, V is the volume of the material, B is the magnetic field, and μ_0 is the permeability of free space.

To achieve stable levitation, the potential energy of the diamagnetic material in the magnetic field must have a minimum, which means that the magnetic susceptibility of the material and its surrounding medium must satisfy the condition:

$$\chi_s - \chi_m < 0 \tag{4.3}$$

where χ_s is the magnetic susceptibility of the surrounding medium. This condition ensures that the potential energy of the diamagnetic material in the magnetic field is minimized at the center of the field, where the force of the magnetic field is balanced by the force of gravity.

4.3 Magneto-Archimedes Levitation

4.3.1 Principle

As we discussed before, samples can be levitated stably using magnetic field when $\chi_s - \chi_m < 0$. Thus, the study of weakly magnetic samples $(|\chi| \leq 10^{-5})$, which are typically considered "non-magnetic", suspended in paramagnetic environments has become increasingly widespread. This technology utilizing the magnetic buoyant force to stable the sample and the buoyant force from surrounding medium to provide the enormous force to against gravity, is widely called "Magneto-Archimedes levitation". The concept "Magneto-Archimedes levitation" was firstly proposed by Yasuhiro Ikezoe in 1998 [3]. They utilized the gravitational and magnetically induced buoyancy forces in the host paramagnetic atmosphere (i.e., pressurized oxygen) to balance the gravitational force on the levitating object. By increasing the pressure of the gaseous paramagnetic medium, there are two main benefits: (i) the buoyant force is increased due to the density increasement of the surrounding medium; and (ii) the magnetic susceptibility of the paramagnetic atmosphere is significantly strengthened, since there is more paramagnetic oxygen gas molecule in a unit volume, i.e., the ratio of magnetic susceptibility between medium and object (water) was boosted from ~0.042 to ~2.5 at 60 atm. Through this method with both buoyancy force and magnetic force enhanced, the requirement to the magnetic field, i.e., magnetic source, can be enormously reduced, resulting in the wide application of permanent magnet instead of superconducting electromagnet (Fig. 4.1).

The magnetic force F_m and Archimedes buoyant force F_b acting on the object surrounded by paramagnetic medium can be given by:

$$\vec{F}_m + \vec{F}_b = \frac{\chi_s - \chi_m}{\mu_0} V_s \left(\vec{B} \cdot \nabla \right) \vec{B} + (\rho_s - \rho_m) V_s \vec{g} \tag{4.4}$$

where subscript s and m represent the object and paramagnetic medium, χ is the magnetic susceptibility, ρ is the density, V_s is the volume of object, $\vec{B}$ is the magnetic field, and $\vec{g}$ is the gravitational acceleration. Based on this equation, Magneto-Archimedes levitation can be realized using a magnetic field source to produce magnetic field strength and gradient $\left(\vec{B} \cdot \nabla \right) \vec{B}$ once the magnetic susceptibility and density of the surrounding paramagnetic medium is sufficient to satisfy $\vec{F}_m + \vec{F}_b = 0$.
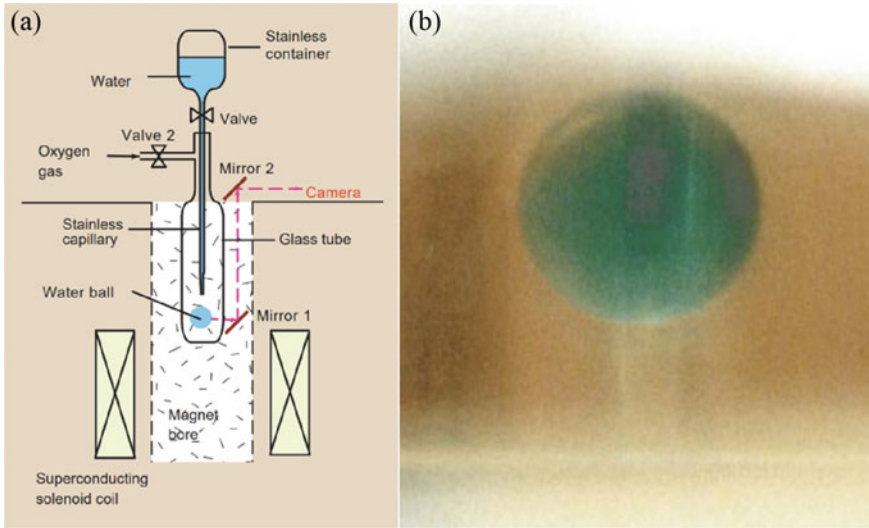
Fig. 4.1 **a** Schematic and **b** picture of levitating water in a superconducting solenoid. Reproduced with permission from Ref. [3]. Copyright 1998 Springer Nature

Before Magneto-Archimedes levitation is proposed, scientists always utilized strong magnetic field source, i.e., superconducting electromagnet, to produce extremely high magnetic field (>10 T) to achieve diamagnetic levitation. With the help of paramagnetic medium, the requirement for magnetic source is significantly reduced and permanent magnets is able to levitate weakly magnetic objects.

4.3.2 Paramagnetic Medium

The utilization of denser solutions has been discovered to enhance the buoyancy experienced by the sample, thus partially counteracting the force of gravity. Moreover, the use of a paramagnetic medium with higher magnetic susceptibility can amplify the magnetic force acting on the sample under similar circumstances. Common paramagnetic media with elevated magnetic susceptibilities include metal salt solutions containing ions such as Mn^{2+}, Gd^{3+}, and Dy^{3+} [8]. These paramagnetic solutions are easily prepared and stored, possess stable chemical properties, and are suitable for diverse applications. As a result, the development of new paramagnetic solutions has reduced the reliance on magnetic suspension systems that necessitate high field strength and gradient, enabling the employment of low-strength electromagnets or even permanent magnets in Magneto-Archimedes levitation technology.

The research implications of this advancement primarily include density measurements of weakly magnetic materials and non-contact magnetic manipulation of

suspended samples. For instance, in 2002, Yamato et al. employed a < 10 T super-conducting electromagnet alongside a high-concentration $MnCl_2$ aqueous solution at 70 °C under atmospheric pressure to achieve real-time observation of the polymerization process of benzyl methacrylate, a high polymer. The stable position of the material in the magnetic field changed due to variations in properties, particularly density and magnetic susceptibility, during the polymerization process. This study also demonstrated the potential of magnetic control to alter the position of suspended samples by adjusting the magnetic field strength [9]. In 2004, Maki et al. used a 3.8 T electromagnet and $GdCl_3$ to achieve high-quality lysozyme crystallization, as depicted in Fig. 4.2, where crystals grown in the suspended state exhibited improved orientation and fewer macroscopic defects [10]. Furthermore, in 2005, Yakayama et al. employed a 4.87 T magnetic field and a 40 wt% $MnCl_2$ solution to suspend and self-assemble gold particles, observing a phenomenon similar to crystallization by introducing a paramagnetic medium to amplify the magnetic force between particles [11]. In 2004, Winkleman et al. constructed a magnetic suspension device with a substantial magnetic field gradient using a permanent magnet magnetic tip [12] and combined it with a low-concentration Gd·DTPA solution to create a biocompatible paramagnetic medium for capturing and manipulating cell particles. This demonstrates the gradual shift in the composition of magnetic suspension systems from superconducting electromagnets to permanent magnets, significantly reducing the requirements for employing Magneto-Archimedes levitation technology. The combination of permanent magnets and paramagnetic solutions has expanded the range of applications for magnetic suspension technology.

The initial magnetic susceptibility of paramagnetic solution is given by:

$$\chi_m = \frac{\mu_0 n m_{eff}^2}{3k_B T} + \chi_{solvent} \tag{4.5}$$
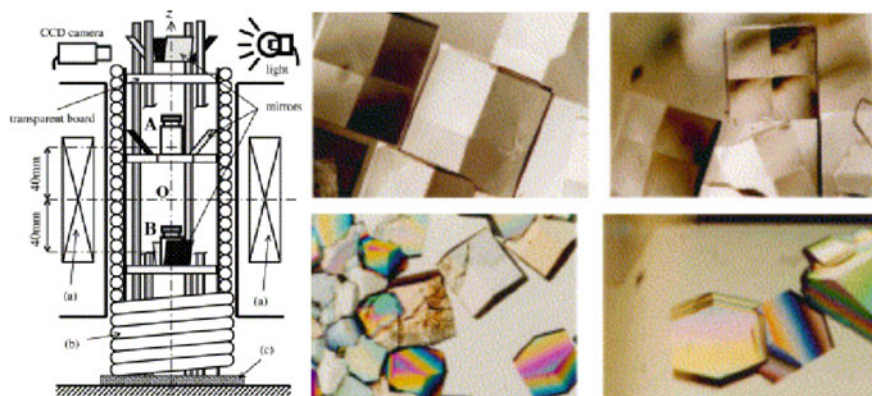

Fig. 4.2 Early applications of magnetic levitation technology: high-quality crystal growth in an electromagnetic coil device. Reproduced with permission from Ref. [10]. Copyright 2004 Elsevier

Table 4.1 Effective magnetic moment of different ions [13]

Ion	Number of unpaired electrons	m_{eff}/μ_B
Ti^{3+}	1	1.73
Ni^{2+}	2	2.8–3.5
Cr^{3+}	3	3.70–3.90
Fe^{2+}	4	5.1–5.7
Mn^{2+}	5	5.65–6.10
Fe^{3+}	5	5.7–6.0
Ga^{3+}	7	8.9
Dy^{3+}	5	10.6

where n is the number density of the ions or particles, m_{eff} is the effective magnetic moment of the paramagnetic salt ion, k_B is Boltzmann constant, T is temperature, $\chi_{solvent}$ is the bulk magnetic susceptibility of the solvent. For paramagnetic salts, m_{eff} is usually expressed in multiples of Bohr magnetons, $\mu_B \approx 9.27 \times 10^{-24}$ J/T, which is used to describe the magnetic properties of electrons in atoms and molecules, particularly their interaction with external magnetic fields. Typical metal ions and their effective magnetic moments are listed in Table 4.1. There are two drawbacks when employing paramagnetic salt solution as medium: (i) the highest concentrations attainable of these ions are typically less than 5 mol/L, corresponding to magnetic susceptibility of e.g., $\chi_m = 1.77 \times 10^{-3} - 9 \times 10^{-6} \approx 1.77 \times 10^{-3}$ for 3 M Dy^{3+} solution at room temperature ($T = 300$ K); (ii) highly concentrated paramagnetic salt solutions are toxic for living matter, such as cells and tissues, limiting their applicability in biological levitation.

Magnetic nanoparticle dispersions, i.e., magnetic fluid or ferrofluid, containing superparamagnetic nanoparticles (NPs) provide an intriguing alternative due to their considerably high magnetic moment and capacity for tailoring surface chemistries in order to achieve compatibility with living cells. Specifically, an iron oxide nanoparticle with an effective diameter of 5 nm shows effective magnetic moment of ca. 3400 μ_B. These high values suggest that a much lower concentration of NPs can be used to achieve the same level of susceptibility as paramagnetic salt solutions. However, it is important to note that superparamagnetic nanoparticles saturate at much lower fields compared to ionic solutions. In an ideal scenario, there are no intermolecular interactions, such as dipole–dipole interactions or van der Waals forces, between the magnetic nanoparticles in a magnetic fluid, i.e., there is no aggregation observed among these nanoparticles. In this ideal case, the magnetic fluid can be considered as a single system consisting only of individual particles. The magnetization intensity of the magnetic fluid can be effectively described using the Langevin function model.

$$M = nm_{eff}\left(\coth x - \frac{1}{x}\right) \tag{4.6}$$

where $x = \frac{m_{eff}\mu_0 H}{k_B T}$.

In addition, it is necessary to consider the influence of thermal fluctuations on the suspension of magnetic nanoparticles under strong field gradients, unlike paramagnetic salts which do not face this issue. A rough estimate can be obtained by comparing the magnetic energy of a fully magnetized and comparing this value to thermal energy. Gerber et al. [14] have developed the following criterion to estimate its diameter D_p:

$$|F|D_p \leq k_B T \tag{4.7}$$

where $|F|$ is the magnitude of t he total force acting on the particle. For the Fe_3O_4 particles in water, the threshold diameter is $D_p = \frac{k_B T}{|F|} = 40$ nm [15]. Larger particles will partially migrate towards the high-filed regions near magnetic sources. The manipulation of cells and other biological materials requires careful consideration of surfactants, pH value, and ionic strength when using ferrofluids to ensure biocompatibility. It is crucial to maintain a pH value of approximately 7, and the nanoparticle materials must be non-toxic to cell cultures. Additionally, it is important to maintain colloidal stability to ensure the viability of live cells. However, one limitation of ferrofluids is their opacity, which can make observation challenging unless a fluorescent dye is used.

4.3.3 Required Magnetic Field

The successful application of Magneto-Archimedes levitation heavily depends on the magnetic field. As mentioned earlier, the use of a high-density paramagnetic liquid medium significantly reduces the necessary magnetic field and field gradient to BdB/dz $= 420$ T^2/m. This enables the levitation of samples using the magnetic field generated by permanent magnets. Nevertheless, it is crucial to carefully construct an appropriate magnetic field to achieve stable sample suspension. In a magnetic field, there must be a place satisfying $\nabla^2 B^2 \geq 0$, i.e., the stable levitation point. Before employing the Magneto-Archimedes levitation, it is necessary to find out whether the manipulation/levitation region has the stable levitation, i.e., the minimum magnetic potential value for diamagnetic object. Therefore, choosing an adequate magnetic field is the key to Magneto-Archimedes levitation.

Here, taking single rectangular magnets for example, spatial magnetic field above a series of square magnets with various length to heigh ratio ($a/b = 0.5$–2) are simulated using COMSOL Multiphysics and shown in Fig. 4.3. The grade designation of the magnet is N52, indicating the remanence ranges from 1.42 to 1.48 T (T). From the simulation results, two points can be observed: (1) There will always be a region of minimum values on the surface of the magnet; (2) As the length/height ratio increases, the range of usable minimum value regions also increases. Certainly, for magnets with the same height, increasing the surface area of the magnet pole will lead to a decrease in the magnetic field gradient, thus reducing the strength of the magnetic field force. On the other hand, if a magnet with a smaller pole area, commonly
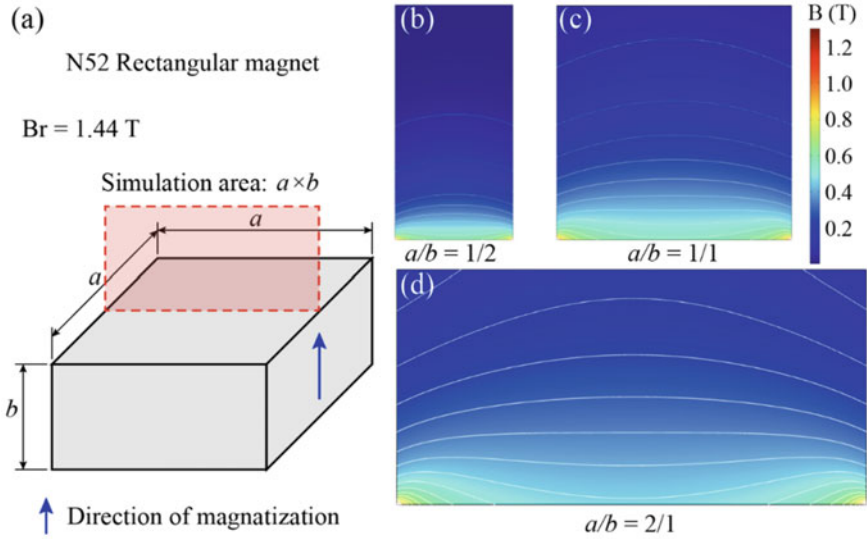
Fig. 4.3 Simulation of the magnetic field distribution above a N52 rectangular magnets. **a** Schematic of magnet, and simulation results of magnets with length/height ratio of **b** $a/b = 1/2$; **c** $a/b = 1/1$; **d** $a/b = 2/1$

known as a magnetic needle, is chosen, it can generate considerable magnetic force for particles. However, due to its limited range of effect, the overall range of stable levitation is also greatly restricted. This result provides us with some preliminary insights for designing the desired magnetic field: for magnets with the same height, a smaller pole area can generate a larger magnetic field force, but the operational area is also smaller, and vice versa.

4.4   Levitation Feature

4.4.1   Levitation Height

There are two main forces acting on the levitating object in the paramagnetic medium: Magnetic buoyant force F_m, and buoyant force F_b. The former magnet exhibits a magnetic field in all directions, while the latter magnet only exerts a force in the direction of gravity. In a Cartesian coordinate system, a suspended sample must satisfy the conditions $F_{mx} = F_{my} = 0$, and $F_{mz} = F_b$. The magnetic buoyant force varies at different positions within the magnetic field. Typically, for square magnets and circular/ring magnets, the stable suspension position is located along a vertical line passing through the center of the surface. Nevertheless, at different locations along this line, the experienced Fmz differs. Thus, considering Eq. 4.4, it becomes

evident that, apart from the magnetic source, factors such as solution density and the magnetization of both the solution and the sample influence the suspension height.

Here taking single ring magnet as an example, as shown in Fig. 4.4 [16]. Two kinds of ring magnet with axial magnetization are used to create the magnetic field, i.e., N35-H20 (inner radius $r_1 = 20$ mm, outer radius $r_2 = 30$ mm, height $h = 20$ mm, and surface magnetic pole density $\sigma = 1.23$ T) and N35-H10 ($r_1 = 12.5$ mm, $r_2 = 25$ mm, $h = 10$ mm, and $\sigma = 0.88$ T). Under the influence of a gradient magnetic field in the axial direction, the diamagnetic objects (e.g., cells, carbon materials, and polymers) immersed in the paramagnetic solution will be relocated at an equilibrium levitation position along the centerline of the magnet (Fig. 4.4a). The transparent paramagnetic solutions allow a good visualization of the submerged objects.

The magnetic force that is applied on a diamagnetic object around the N35-H20 ring magnet (provided by Jiuci Magnets, Inc., Beijing, China) can be calculated. In the blue region in Fig. 4.4a, the diamagnetic object in the tube is forced to move away from the centerline of the magnet, while the object is forced to move along with the
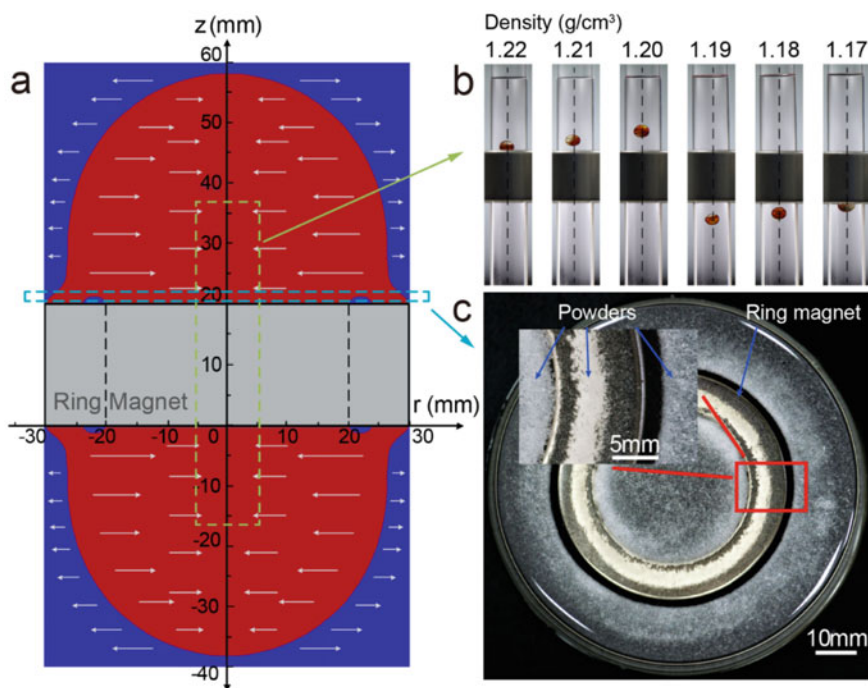

Fig. 4.4 Magnetic force acting on a diamagnetic object around the ring magnet. **a** Plot illustrating the direction of the horizontal force in the r-z plane surrounding the N35-H20 ring magnet. The red region indicates the horizontal force directed towards the centerline, while the blue region represents the reverse direction. **b** Plot of levitating object ($\rho_s = 1.1700 - 1.2200$ g/cm^3) along the centerline in 2.0 M MnCl$_2$ aqueous solution. **c** Plot of distribution of highly dense powders (microcrystalline cellulose, diameters ~80 μm) at a distance of 1 mm from the upper surface of the ring magnet. Reproduced with permission from Ref. [16]. Copyright 2022 American Chemical Society

centerline in the red region. This finding explains the phenomenon that the object assembles along the centerline, see in Fig. 4.4b. As shown in Fig. 4.4a, a unique pattern of the magnetic force that applied on the surface of the ring magnet can be found: the force drives the object to move away from the centerline in the semi-circular blue region, while the object is forced towards the centerline in the red region. Microcrystalline cellulose powders (purchased from Sinopharm Chemical Reagent Co., Ltd, Beijing, China) are used to verify this phenomenon. The microcrystalline cellulose powders are of higher density ($\rho_s = 1.605$ g/cm^3), and consequently, they subside on the upper surface of the ring magnet. The ring magnet configuration exhibited that high-density powders can be dispersed around the inner and outer rings of the magnet, as shown in Fig. 4.4c. This distribution of the powders is consistent with the pattern of the magnetic force distribution (see Fig. 4.4a). The proposed mathematic model improves the understanding of the single ring Magneto-Archimedes levitation. In Fig. 4.4b, standard density beads with different densities ($\rho_s = 1.1700$ –1.2200 g/cm^3) are levitated along the centerline in 2.0 M MnCl$_2$ aqueous solution. The levitation height varies with the bead's density. The experiment results are consistent with the calculation results. According to Eq. 4.4, once the magnetic field and paramagnetic medium are established, the levitation height is primarily influenced by the magnetic susceptibility and density of the object. However, it is worth noting that the density plays a more prominent role due to the minimal variations in magnetic susceptibility among different materials.

Glass beads of standardized densities (1.1200–1.3500 $\pm$ 0.0002 g/cm^3, purchased from American Density Materials, Inc., Staunton, VA, USA) are tested using different solutions and magnets, and the experiments are performed at an ambient temperature of 23 °C. Figure 4.5 shows the actual density values (dots) and calculated results (lines) under two different magnets (N35-H20 and N35-H10) using 1.5 M, 2.0 M, 2.5 M and 3.0 M MnCl$_2$ aqueous solutions. From Fig. 4.5, it can be seen that the calculated curves show a good agreement with the actual values of these standardized density glass beads. These results confirm the effectiveness of the derived density measurement equation under different magnets and different paramagnetic solutions. The ring magnets in Fig. 4.5a, b were N35-H20 and N35-H10, respectively. A unified mathematic model is necessary to precisely correlate the density, magnetic field and levitation height. The proposed configuration can be used with ring magnets of any size. Aside from changing magnets, it can also be found that changing solutions could alter the ranges and sensitivity of density measurement of the configuration. As shown in Fig. 4.5a, choosing paramagnetic solutions with higher concentrations will yield a higher measurement range; $\rho_s = 1.1258$–1.1706 g/cm^3 in 1.5 M solution, while $\rho_s = 1.2461$–1.3379 g/cm^3 in 3.0 M solution. Similarly, a higher sensitivity can be achieved using paramagnetic solutions of lower concentrations. In sum, through changing solutions or magnets, the proposed configuration can be employed in various scenarios where a wider density measuring range or a higher sensitivity is required.
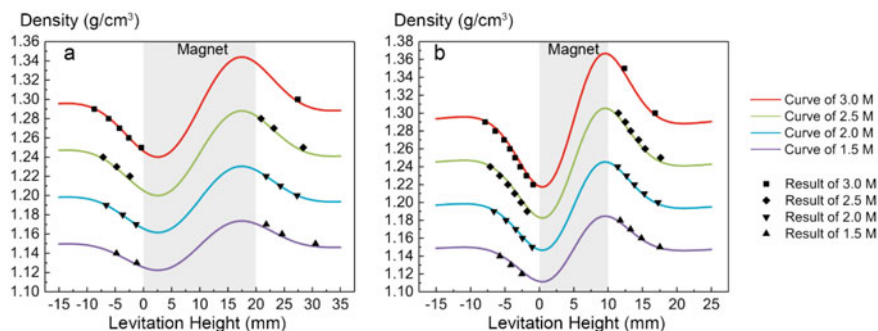
Fig. 4.5 The experimental results and actual densities in 1.5 M, 2.0 M, 2.5 M and 3.0 M MnCl$_2$ aqueous solutions. **a** The measurements of different standard density glass beads using the N35-H20 ring magnet. The view of the gray region is blocked by the ring magnet. **b** The measurements of different standard density glass beads using the N35-H10 ring magnet

4.4.2 Levitation Posture

Magneto-Archimedes levitation is capable of suspending, localizing, and orienting an object without the need for contact with a solid surface, such as a gripper or solid wall, by carefully balancing gravitational and magnetic forces. When subjected to an applied magnetic field, it has the ability to levitate various diamagnetic materials in a paramagnetic medium. This method is widely available and offers high density resolution and portability. Numerous studies have demonstrated the effectiveness of Magneto-Archimedes levitation in analyzing forensic evidence, food, minerals, and other substances [17–19]. Furthermore, the principles of Magneto-Archimedes levitation have been applied to various fields, including 3D cell culture [20], separation of mixed waste [21], and self-assembly [22]. In addition to using the levitation height of an object for density measurement, the levitation posture can also be utilized for defect detection within the object. It is important to consider the object's shape rather than simplifying it as a particle when employing the levitation posture for detection. The imbalance between magnetic force and buoyancy can result in a non-horizontal levitation posture due to variations in density among different parts of an axisymmetric object. By combining the theoretical model for spatial magnetic field distribution with the levitation posture, internal defects can be detected using the Magneto-Archimedes levitation method in a matter of seconds.

Xie et al. [23] established a theoretical model to demonstrate the influence of different distances between the two magnets on the linear relationship of the device. The model explains the phenomenon of samples assembling along the centerline. In another study, Xia et al. [24] utilized the Magneto-Archimedes levitation method to diagnose internal voids in 3D printed parts, highlighting its potential for non-destructive product testing. Gao et al. [25] proposed a dynamically rotating MagLev method to amplify the interior differences in objects of different density distribution, and characterizes the spatial density heterogeneity of the levitation objects.

The use of the rotating-mode density measurement method with magnetic levitation shows promise for offering a straightforward operational approach to separate and perform quality control on objects with varying shapes in materials science and industrial applications. Tang et al. [26] proposed a non-destructive measurement based on the Magneto-Archimedes levitation method for analyzing internal defects in plastic gears by its levitation posture. The experimental results demonstrate that the calculated porosity level has an average relative error of less than 7%. Additionally, the theoretical model for the distribution of shrinkage voids aligns well with the results obtained through CT detections, with a correlation coefficient of up to 99.8%. These findings indicate that the proposed method holds immense potential for mass detection of plastic gears.

For instance, the presence of shrinkage voids in plastic gears leads to density variations; higher numbers of shrinkage voids correlate with lower densities compared to samples with fewer voids. In general, when the mass of plastic gears remains constant, there is a linear relationship between the porosity levels and the reciprocal of the sample density, as outlined by Eq. 4.8:

$$\eta = f(\rho_s) = k\frac{1}{\rho_s} + b \tag{4.8}$$

where η is the porosity level of the sample, k and b are the coefficients that are determined by the chosen samples with the maximum and minimum porosity levels. Through Eq. 4.8, the porosity levels of defective samples in a certain interval can be measured through the Magneto-Archimedes levitation method without CT detection.

To establish the relationship between levitating posture and the distribution of shrinkage voids in plastic gears, the principle of minimum potential energy [27]. Equation 4.9 represents the total energy of a sample levitating in a magnetic field, where $\boldsymbol{r_{cm}} = (\boldsymbol{i_{cm}}, \boldsymbol{j_{cm}}, \boldsymbol{k_{cm}})$ represents the center of mass, which may deviate from the centroid of the sample due to the presence of non-uniform shrinkage voids. Additionally, $\overrightarrow{e_z}$ denotes the unit vector along the z-axis. When the sample achieves an equilibrium state with a specific posture, the total energy should be minimized. Equation 4.10 illustrates the energy associated with different sample postures, where θ is the tilt angle of the sample, and λ_l denotes the lengths of principal axes calculated by $\lambda_l^2 = \frac{1}{V}\int_V l^2 dV$ for $l \in \{i, j, k\}$. These principal axes affect the final posture of the sample in the magnetic field. Given the plastic gear's symmetrical nature, resembling a hollow cylinder, it is practical to select the principal axes wherein the center of mass r_{cm} always lies on the i-axis, as $(i_{cm}, 0, 0)$.

$$U = U_{mag} + U_{grav} = -\int_V \left(\frac{\Delta\chi}{2\mu_0}\vec{B} \cdot \vec{B} + \Delta\rho \mathrm{g}r_{cm} \cdot \overrightarrow{e_z}\right)dV \tag{4.9}$$

$$U(\theta) = -\frac{2B_0^2\Delta\chi V}{\mu_0 d^2}\left(\lambda_i^2 - \lambda_k^2\right)\cos^2\theta - \rho_s V \mathrm{g}i_{cm}\cos\theta \tag{4.10}$$

The random nature of the distribution of shrinkage voids within the plastic gear makes it challenging to determine the position and volume of each void. To quantify the distribution of shrinkage voids, a new variable called the moment of volume M_v is introduced, which is analogous to the moment of force in mechanics. Previous research [22] has shown that larger volumes of voids and greater distances from the centroid of the sample both contribute to an increased tilt angle of the sample. Equation 4.11 illustrates the relationship between the tilt angle θ and the moment of volume M_v for the deflection of the plastic gears.

$$M_v = V_{total}L_i = -\frac{4B_0^2 \Delta\chi V\left(\lambda_i^2 - \lambda_k^2\right)}{\mu_0 g d^2 (\rho_r - \rho_v)} \sin\theta \qquad (4.11)$$

where V_{total} represents the total volume of shrinkage voids, and L_i represents the distance between the centroid of shrinkage voids and the central point of the sample, which is situated along the body-fixed i-axis to facilitate computation. ρ_v and ρ_r are the density of shrinkage voids and parts without shrinkage voids of sample, respectively. From Eq. 4.11, the distribution of the shrinkage voids can be quantified.

4.5 Axial Levitation

The current applications of Magneto-Archimedes levitation method are briefly discussed in the above sections, and they primarily utilize the principle of levitation along the centerline, i.e., axial levitation. However, how can we determine whether the sample in the device is effectively suspended along the center line based on the magnetic field?

When a sample is placed in a paramagnetic medium within a Magneto-Archimedes levitation device, its vertical motion is influenced not only by the magnetic force but also by the differences in gravitational and buoyant forces experienced by different samples. Therefore, it is necessary to conduct stability analysis in the horizontal direction first in order to determine the stable region of horizontal movement. This analysis involves examining the horizontal movement trend of the sample under the influence of the horizontal magnetic field force. Once the stable region in the horizontal direction has been identified, the vertical magnetic force within that region is analyzed to determine the conditions for stable levitation and to identify the stable levitation position for different samples within the circular magnet device.

Here, taking axial levitation in a two-ring-magnet configuration as an example (Fig. 4.6a). When a sample is placed in the Magneto-Archimedes levitation device, it is subject to magnetic field forces in both horizontal and gravitational direction. When the sample is stably levitated, the horizontal magnetic force becomes 0 and the gravitational magnetic force is equal to the gravitational and buoyant forces. Therefore, for a sample to be stably levitated, the magnetic force it experiences in the horizontal direction must be equal to zero, as shown in Eq. 4.12. However, this is not

enough; in addition to a zero magnetic field force, the sample also needs the ability to resist disturbances to achieve stable levitation. The direction of the horizontal component of the magnetic force should point towards the stable point on both sides of the stable region, as shown in Fig. 4.6b. The figure presents a two-color plot of the horizontal component of the magnetic force on a single ring magnet. The red color indicates that the force points in the negative direction of the r-axis, while the blue color indicates that the force points in the positive direction of the r-axis. The yellow line in the figure represents the region where the magnetic force is zero. A horizontal line segment is selected near the surface of the magnet ($z = 21$ mm) and away from the surface of the magnet ($z = 30$ mm) for analysis. The five points (numbered in the figure) where the line segment intersects with the yellow line are the points where the magnetic force is zero on the line segment. Based on the analysis of the plot, it can be determined that points #1, #3, and #5 have their horizontal component of the magnetic force pointing towards the respective points. This indicates that the sample can be in a stable state in the horizontal direction when located at these three points. From a numerical analysis perspective, for stable levitation in the horizontal direction, the magnetic force on both sides of the stable point should point towards the stable point, i.e., the horizontal component of the magnetic force should satisfy Eq. 4.13. Therefore, combining Eq. 4.12, it can be seen that all values inside the magnetic force formula, except for the magnetic field intensity, are constant. Furthermore, since the magnetic susceptibility of paramagnetic media is always greater than that of the sample, i.e., $\chi_s - \chi_m < 0$, it is sufficient to satisfy Eq. 4.14 for the horizontal component of $\left(\vec{B} \cdot \vec{\nabla} \right) \vec{B}$ to find the stable region of the sample in the Magneto-Archimedes levitation device.

As shown in Fig. 4.6c, d, numerical calculations were performed on the selected line segment's $B_r(\partial B_r/\partial r) + B_z(\partial B_r/\partial z)$ (red line) and its derivative (blue line). The five selected points were also marked in the figure. For points #2 and #4, although they satisfy $B_r(\partial B_r/\partial r) + B_z(\partial B_r/\partial z) = 0$, their corresponding derivatives are both less than zero. This indicates that these two points do not satisfy the condition of Eq. 4.14 and therefore cannot achieve stability in the horizontal direction. In contrast, points #1, #3, and #5 satisfy Eq. 4.14 and can achieve stability. This is consistent with the results from the analysis of the plot, demonstrating the importance of the mathematical model in Magneto-Archimedes levitation theory.

$$F_{\text{mag},r} = \frac{\chi_s - \chi_m}{\mu_0} V \left(B_r \frac{\partial B_r}{\partial r} + B_z \frac{\partial B_r}{\partial z} \right) = 0 \tag{4.12}$$

$$\frac{d F_{\text{mag},r}}{dr} < 0 \tag{4.13}$$

$$B_r \frac{\partial B_r}{\partial r} + B_z \frac{\partial B_r}{\partial z} = 0 \quad \text{and} \quad d \left(B_r \frac{\partial B_r}{\partial r} + B_z \frac{\partial B_r}{\partial z} \right) / dr > 0 \tag{4.14}$$
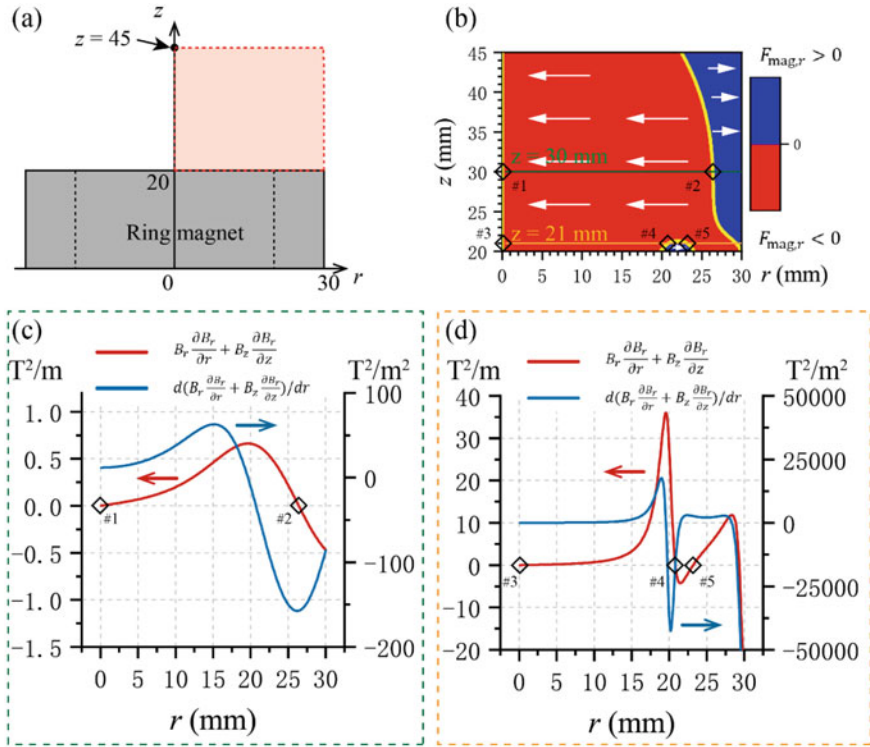
Fig. 4.6 Calculation of horizontal stability in the levitation condition **a** schematic of the analysis region **b** two-dimensional graph of the horizontal component of magnetic force **c** numerical analysis of the horizontal stability state at z = 30 mm **d** numerical analysis of the horizontal stability state at z = 21 mm

4.6 Circular Levitation

The ability to detect small differences in density is crucial for achieving precise measurements of the shape and properties of precision products. The ring magnet device offers various advantages in density measurement, including high accuracy, a large operational and observation space, low cost, and rapid measurement. Similarly, the two-magnet device allows for high sensitivity measurements by adjusting the spacing between the magnets. However, a limitation shared with the rectangular opposing magnet configuration [28] is that increasing the spacing between the magnets causes the sample to be suspended unstably and pushed away from the centerline. This constraint restricts traditional magnetic levitation devices when attempting to achieve high sensitivity density measurement through increased spacing between magnets. Existing high-sensitivity density measurement methods also fail to ensure a comprehensive density measurement range. Furthermore, in current magnetic levitation methods, stable sample suspension can only be achieved

within a one-dimensional linear structure along the centerline. This constraint leads to mutual compression among samples with small density differences during density measurement or sample separation, thereby affecting the suspension effect. As a result, the axial levitation method often faces limitations when conducting batch density characterization.

Here, taking magneto-levitation device consisting of two H20 magnets with same poles facing each other as an example. The two-ring-magnet device can achieve axial levitation when the spacing is small ($d < 32$ mm). The measurement sensitivity can vary depending on the spacing, reaching its maximum at $d = 32$ mm. However, when the spacing is greater than 32 mm, due to the presence of a non-zero horizontal component of the magnetic force on the sample, with the magnetic force pointing towards the outer region, the sample cannot stably levitate along the center line. Consequently, the device loses its capability for axial levitation, similar to rectangular magnet devices [23]. However, the ring magnet device differs in that, after analyzing the magnetic field and its distribution, it is observed that the stable levitation region is not limited to the center line but rather forms a stable circular levitation region. Taking the dual-block H20 magnet device as an example with a spacing of $d = 33$ mm, the calculated results are shown in Fig. 4.7. Considering the green line segment (z = 28 mm) as an example, horizontal force analysis of the non-axial levitation region in the figure reveals the presence of points where stable levitation can still be achieved in the outer region, such as point #1. This indicates that stable levitation can be realized along the yellow segment in Fig. 4.7a. Moreover, an analysis of the vertical stability conditions for this region shows compliance with the conditions, as shown in Fig. 4.7b. Hence, it can be concluded that although increasing the spacing in the device prevents continuous axial levitation of the internal sample, it allows for stable levitation in the corresponding circular region. Additionally, due to the axial symmetry of the magnetic field generated by the ring magnet, it can be inferred that this stable levitation region forms a circular levitation structure, which is different from any existing magnetic levitation structures. This method breaks the requirement of "axial levitation" in existing magnetic levitation techniques and achieves stable sample levitation in cases where the spacing is large, constructing a stable circular levitation region. This also enhances the research value and application prospects of ring magnet devices in the field of magnetic levitation.

To utilize the ring magnetic levitation method for density measurement, it is important to consider the operational procedure of the magnetic levitation method. In this procedure, the sample to be measured is placed in a container aligned coaxially with the ring magnet. The sample is positioned slightly below the lower surface of the upper magnet. As a result, under the influence of magnetic field forces, the sample will automatically find its balance at the corresponding levitation point. It is important to note that the annular levitation region exists in the middle part of the device (between the two yellow regions), rather than being comprised solely of the two separate regions shown in Fig. 4.7a. In density measurement using the dual ring magnet setup, which follows the "up small and down large" measurement range, we further increase the spacing to $d = 40$ mm, as shown in Fig. 4.8 [28]. For ease of comparison, the "red-blue gradient" color map is changed to a "green–brown
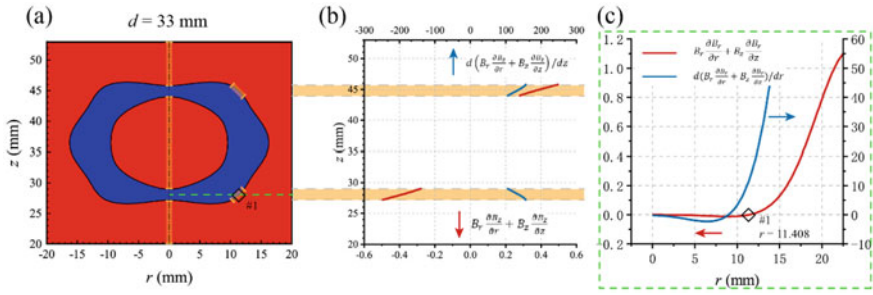
Fig. 4.7 Analysis of stable levitation of the two-ring-magnet device with a large distance ($d = 33$ mm). **a** Contour plot of the horizontal component of the magnetic force. **b** Analysis of vertical stability within the region. **c** Analysis of horizontal stability within the region

gradient". When the sample is levitated in a lower region (IV or V region), it will inevitably traverse through an outward horizontal force region (II region) within the vertical force effect during the balancing process. The magnitude of the magnetic force is linearly correlated with $\left(\vec{B} \cdot \vec{\nabla}\right)\vec{B}$, considering a specific sample and solution. Therefore, as the sample passes through the II region, where the horizontal outward force is relatively large, it will be pushed towards a stable region outside the centerline. This is indicated by the outer black dashed line in Fig. 4.8a. If the levitation height of the sample corresponds to the IV region, its stable point will still align with the black dashed line. On the other hand, if the sample's levitation region is in the V region, after descending to the corresponding height, it will experience an inward horizontal component of magnetic force in that region. As a result, the sample will continue to levitate along the center line. In the case of the III region, despite the existence of stable conditions for axial levitation in that region, the operational procedure for sample density measurement involves balancing from top to bottom. Therefore, the horizontal component of magnetic force exerted on the sample in the II region is relatively substantial. Consequently, the stable levitation region at the corresponding height in the III region will still be defined by the outer dashed line. Based on the aforementioned analysis, it can be inferred that in an annular levitation setup with a large spacing, the stable region for sample levitation will inevitably be defined by the red dashed line in the upper right corner of Fig. 4.8a. This implies axial levitation on both the upper and lower sides (I and V regions), while the middle section remains stably levitated beyond the center line. The axial symmetry of the ring magnet setup results in a corresponding axial symmetry in the stable region outside the center line. Consequently, samples of the same density exhibit a ring-shaped levitation structure during the levitation process, as depicted in Fig. 4.8b. This figure illustrates the schematic diagram of batch sample levitation in a ring magnet setup with a spacing of 40 mm. It is evident that the levitated samples, influenced by the horizontal component of the magnetic field force, are pushed beyond the center line, forming an annular levitation structure. In the stable levitation state, the sample only possesses a vertical component that balances gravity and buoyancy.
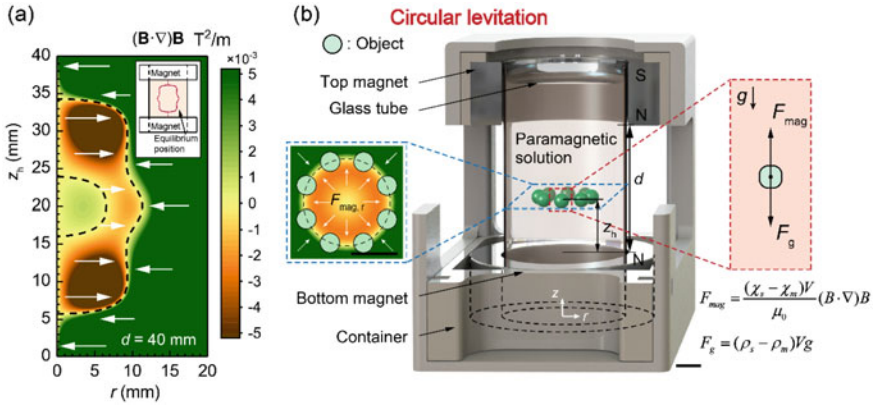
Fig. 4.8 Circular levitation structure in the two-ring-magnet device at d = 40 mm **a** contour plot of the horizontal component of the magnetic force. **b** Schematic diagram of the device. Reproduced with permission from Ref. [29]. Copyright 2020 American Chemical Society

In order to accurately determine the levitation position (r, z) for samples levitating in the circular region, the observed data of the sample's levitation height z from a frontal view is necessary. This is because the levitation position directly affects the calculation of the vertical component of the magnetic force acting on the sample. When samples levitate along the center line, the levitation position can be easily confirmed as r = 0. However, for samples levitating in the circular region, the horizontal position r cannot be determined solely through observation. Therefore, it is essential to compute the point that satisfies the horizontal stability condition mentioned in Eq. 4.14 at the given height z in order to determine the horizontal position r. Then the density of levitating sample can be calculated accurately.

References

1. Simon MD, Heflinger LO, Geim AK. Diamagnetically stabilized magnet levitation. Am J Phys. 2001;69(6):702–13.
2. Geim AK, Simon MD, Boamfa MI, et al. Magnet levitation at your fingertips. Nature. 1999;400(6742):323–4.
3. Ikezoe Y, Hirota N, Nakagawa J, et al. Making water levitate. Nature. 1998;393(6687):749–50.
4. Ikezoe Y, Kaihatsu T, Sakae S, et al. Separation of feeble magnetic particles with magneto-Archimedes levitation. Energy Convers Manage. 2002;43(3):417–25.
5. Hirota N, Kurashige M, Iwasaka M, et al. Magneto-Archimedes separation and its application to the separation of biological materials. Physica B. 2004;346:267–71.
6. Liu J, Ding A, Cao Q. Magnetic levitation with cylindrical magnets for density-based measurement. IEEE Trans Instrument Measur. 2021.
7. Miura O, Yamagishi K, Yamamoto D. Magneto-Archimedes levitation of precious metals under a high magnetic field gradient. J Phys Conf Ser. 2018;1054(1): 012086.
8. CRC handbook of chemistry and physics. CRC Press; 2014.

9. Yamato M, Nakazawa H, Kimura T. Levitation polymerization to fabricate a large polymer sphere. Langmuir. 2002;18(24):9609–10.

10. Maki S, Oda Y, Ataka M. High-quality crystallization of lysozyme by magneto-Archimedes levitation in a superconducting magnet. J Cryst Growth. 2004;261(4):557–65.

11. Takayama T, Ikezoe Y, Uetake H, et al. Self-organization of nonmagnetic spheres by magnetic field. Appl Phys Lett. 2005;86(23):234103.

12. Winkleman A, Gudiksen KL, Ryan D, et al. A magnetic trap for living cells suspended in a paramagnetic buffer. Appl Phys Lett. 2004;85(12):2411–3.

13. Wikipedia contributors. 2023, March 24. Magnetochemistry. In: Wikipedia, the free encyclopedia. Retrieved 07:17, August 25, 2023, from https://en.wikipedia.org/w/index.php?title=Magnetochemistry&oldid=1146373329.

14. Gerber R, Takayasu M, Friedlaender F. Generalization of HGMS theory: the capture of ultra-fine particles. IEEE Trans Magn. 1983;19(5):2115–7.

15. Furlani EP. Analysis of particle transport in a magnetophoretic microsystem. J Appl Phys. 2006;99(2):024912.

16. Zhang C, Zhao P, Gu F, et al. Single-ring magnetic levitation configuration for object manipulation and density-based measurement. Anal Chem. 2018;90(15):9226–33.

17. Bøyum A, Brincker Fjerdingstad H, Martinsen I, et al. Separation of human lymphocytes from citrated blood by density gradient (NycoPrep) centrifugation: monocyte depletion depending upon activation of membrane potassium channels. Scand J Immunol. 2002;56(1):76–84.

18. Xie J, Zhao P, Zhang C, et al. A feasible, portable and convenient density measurement method for minerals via magnetic levitation. Measurement. 2019;136:564–72.

19. Lockett MR, Mirica KA, Mace CR, et al. Analyzing forensic evidence based on density with magnetic levitation. J Forensic Sci. 2013;58(1):40–5.

20. Souza GR, Molina JR, Raphael RM, et al. Three-dimensional tissue culture based on magnetic cell levitation. Nat Nanotechnol. 2010;5(4):291–6.

21. Zhang X, Gu F, Xie J, et al. Magnetic projection: a novel separation method and its first application on separating mixed plastics. Waste Manage. 2019;87:805–13.

22. Mirica KA, Ilievski F, Ellerbee AK, et al. Using magnetic levitation for three dimensional self-assembly. Adv Mater. 2011;23(36):4134–40.

23. Xie J, Zhang C, Gu F, et al. An accurate and versatile density measurement device: magnetic levitation. Sens Actuators B Chem. 2019;295:204–14.

24. Xia N, Zhao P, Xie J, et al. Non-destructive measurement of three-dimensional polymeric parts by magneto-Archimedes levitation. Polym Testing. 2018;66:32–40.

25. Gao QH, Zhang WM, Zou HX, et al. Tunable rotating-mode density measurement using magnetic levitation. Appl Phys Lett. 2018;112(14):142408.

26. Tang D, Zhao P, Shen Y, et al. Detecting shrinkage voids in plastic gears using magnetic levitation. Polym Testing. 2020;91:106820.

27. Subramaniam AB, Yang D, Yu HD, et al. Noncontact orientation of objects in three-dimensional space using magnetic levitation. Proc Natl Acad Sci. 2014;111(36):12980–5.

28. Mirica KA, Shevkoplyas SS, Phillips ST, et al. Measuring densities of solids and liquids using magnetic levitation: fundamentals. J Am Chem Soc. 2009;131(29):10049–58.

29. Zhang C, Zhao P, Gu F, et al. Axial-circular magnetic levitation: a three-dimensional density measurement and manipulation approach. Anal Chem. 2020;92(10):6925–31.